

Reconstruction of single and 2-qubit density matrices using quantum state tomography

Supervisor: Mayerlin Nuñez Portela

Mario Andrés Henao^a, Mateo Restrepo^a

^a*Physics Department - Universidad de los Andes*

Abstract

We report an experimental realization of quantum state tomography of a photonic ensemble for single and two-qubit polarization states. Our implementation is based on the work by James, Kwiat, Munro and White [1] which provides good tomographic reconstructions based on local projective measurements. We describe the theory and experimental tomographic measurement for single qubit states prepared from a laser source and present the tomographic reconstruction of the density matrices of three orthogonal bases. Furthermore, we also describe the theory and experimental realization of a quantum state tomography of the two polarization degrees of freedom of a pair of entangled photons generated in a down-conversion experiment. Two different techniques are discussed: a linear reconstruction, where the density matrix is constructed from coincidence measurements but with the caveat of possibly producing non-physical density matrices, and a maximum likelihood estimation technique that produces physical density matrices. Finally, we also discuss temporal compensation of the down-converted photons in type II BBO crystal and its effect on the tomographic reconstruction of 2-qubit states and present the tomographic reconstruction of the density matrix for an SPDC source.

Keywords: Quantum state Tomography, Quantum process Tomography, Polarization states, qubits, Stokes Parameters, Entanglement.

1. Introduction

Tomography of quantum states is an experimental procedure to determine the quantum state of a system. Thus, a sequence of identical measurements in different bases allow the reconstruction via a maximum likelihood estimation of a complete quantum state. The theoretical ideas for quantum state tomography (QST) were introduced by Fano in 1957 [2]. The first approach towards the determination of the state of a system using tomographic techniques was developed by Vogel and Risken in 1989 [3] for continuous variables. The QST for finite dimensional systems was proposed by Leonhardt in 1995 [4], and is experimentally implemented by measuring the quantum mechanical analogs of Stokes parameters, from which the quantum-polarization state of an ensemble of photonic qubits is inferred. Today QST is the cornerstone of experimental quantum information with quantum systems, especially in quantum computing applications using qubits. QST is used as

Email addresses: ma.henao@uniandes.edu.co (Mario Andrés Henao), m.restrepo11@uniandes.edu.co (Mateo Restrepo)

a benchmark in the quality of entangled photon pairs, and it is widely used to measure polarization entanglement. Entanglement has a remarkable role in quantum optics and quantum information experiments, quantum cryptography and quantum teleportation. Today the most common method for the generation of entangled photon pairs is by means of spontaneous parametric down conversion (SPDC) in non-linear crystals.

In this project, we are interested in using QST to determine the quantum-polarization state of a pair of possibly entangled photons generated by an SPDC optical setup in the quantum optics laboratory. Furthermore, we will gather and statistically analyze the experimental data using computational software such as `Labview` and `Mathematica` in order to do numerical computations and plots.

This project is divided as follows: The first stage consists of understanding and performing a QST to a laser light source (single qubit) prepared into different polarization states with waveplates. The second stage is devoted to understanding and performing a 2-qubit QST to reconstruct the density matrix of an ensemble of possibly entangled photons produced via SPDC in a non-linear crystal.

2. Single qubit quantum state tomography

2.1. Theoretical preliminaries

2.1.1. Polarization

represents a two-level system and is often referred to as a qubit.

In quantum mechanics one says that a vertically polarized photon is in state $|V\rangle$, and in a similar manner $|H\rangle$ represents a horizontally polarized photon, these two states form the basis of a two dimensional Hilbert space. The general polarization state vector of a photon in Hilbert space is written as

$$|\psi\rangle = \cos\left(\frac{\theta}{2}\right) |H\rangle + \sin\left(\frac{\theta}{2}\right) e^{i\varphi} |V\rangle \quad (1)$$

where θ and φ represent the two coordinates on the surface of the *Bloch sphere*, which means that $|\psi\rangle$ lies in the surface of the Bloch sphere [5]. A state like Eq.(1) represents a two-level system and is often referred to as a qubit. Any state generated by combinations of θ, ϕ in Eq.(1) is known as a pure quantum state.

2.1.2. Density Matrix

Hereafter it will be of use to us to use a representation of quantum states known as *density matrix* representation. Such a representation is general and can be applied to both pure a mixed quantum states. A mixed quantum state is defined as an statistical ensemble of *pure states* and can not be described as a ket vector in Hilbert space like Eq.(1). Rather it is described by a density matrix, defined as follows

$$\rho = \sum_s \mathcal{P}_s |\psi_s\rangle \langle \psi_s| \quad (2)$$

where \mathcal{P}_s is the probability of finding each *pure* state $|\psi_s\rangle$ in the aforementioned ensemble. The ensemble expectation value of any observable can be computed using the density matrix of the system in the following way

$$\langle A \rangle = \sum_s \mathcal{P}_s \langle \psi_s | A | \psi_s \rangle = \text{tr}(\rho A) \quad (3)$$

2.1.3. Stokes parameters

Any single qubit state density matrix can be uniquely represented by four parameters, $\{S_0, S_1, S_2, S_3\}$, as

$$\rho = \frac{1}{2} \sum_{i=0}^3 S_i \sigma_i \quad (4)$$

where the σ_i are the standard Pauli matrices plus the identity (σ_0). From Eq.(4) one can compute the value of S_i simply by

$$S_i = \text{tr}(\rho \sigma_i) \quad (5)$$

From the previous relation it follows that:

- $S_0 = 1$.
- For a *pure state* $\sum_{i=1}^3 S_i^2 = 1$.
- For a *mixed state* $\sum_{i=1}^3 S_i^2 < 1$.
- For the maximally *mixed state* $\sum_{i=1}^3 S_i^2 = 0$.

For photon polarization, the appropriately normalized set of S_i are known as the *Stokes parameters*[6].

2.1.4. The photonic case

As we are going to be working with qubit polarization states from a photonic source the following definitions are going to be useful hereafter. A two level photonic system has two basis states, $|H\rangle$ and $|V\rangle$, describing its Hilbert space. Any other *pure* polarization state is constructed from superpositions of these two states. The most common pure states constructed from $|H\rangle$ and $|V\rangle$ are the diagonal, anti-diagonal, right-circular and left-circular. This states are given by the following superpositions:

$$\begin{aligned} |D\rangle &\equiv \frac{1}{\sqrt{2}} (|H\rangle + |V\rangle) \\ |A\rangle &\equiv \frac{1}{\sqrt{2}} (|H\rangle - |V\rangle) \\ |R\rangle &\equiv \frac{1}{\sqrt{2}} (|H\rangle - i|V\rangle) \\ |L\rangle &\equiv \frac{1}{\sqrt{2}} (|H\rangle + i|V\rangle). \end{aligned} \quad (6)$$

And to each of the six states mentioned above corresponds the following density matrix:

$$\begin{aligned}\rho_H &= \begin{pmatrix} 1 & 0 \\ 0 & 0 \end{pmatrix}, & \rho_V &= \begin{pmatrix} 0 & 0 \\ 0 & 1 \end{pmatrix} \\ \rho_D &= \frac{1}{2} \begin{pmatrix} 1 & 1 \\ 1 & 1 \end{pmatrix}, & \rho_A &= \frac{1}{2} \begin{pmatrix} 1 & -1 \\ -1 & 1 \end{pmatrix} \\ \rho_L &= \frac{1}{2} \begin{pmatrix} 1 & -i \\ i & 1 \end{pmatrix}, & \rho_R &= \frac{1}{2} \begin{pmatrix} 1 & i \\ -i & 1 \end{pmatrix}.\end{aligned}\tag{7}$$

Physically the Stokes parameter of a photonic system are given by the outcome of a set of *orthogonal* projective measurements (H/V, D/A, L/R) on the initial state ρ_0 , viz

$$\begin{aligned}S_0 &= \mathcal{P}_{|H\rangle} + \mathcal{P}_{|V\rangle} \\ S_1 &= \mathcal{P}_{|D\rangle} - \mathcal{P}_{|A\rangle} \\ S_2 &= \mathcal{P}_{|L\rangle} - \mathcal{P}_{|R\rangle} \\ S_3 &= \mathcal{P}_{|H\rangle} - \mathcal{P}_{|V\rangle},\end{aligned}\tag{8}$$

where $\mathcal{P}_{|\psi\rangle}$ stands for the probability of projecting state ρ_0 into the the state $|\psi\rangle$, viz

$$\mathcal{P}_{|\psi\rangle} = \langle\psi|\rho|\psi\rangle = \text{tr}(|\psi\rangle\langle\psi|\rho).$$

2.2. Single qubit tomography

In this first stage we use an optical setup consisting of waveplates and polarizers, to perform projective measurements to different prepared polarization states. With the following convention,

$$\begin{pmatrix} 0 \\ 1 \end{pmatrix} = |V\rangle, \quad \begin{pmatrix} 1 \\ 0 \end{pmatrix} = |H\rangle,\tag{9}$$

the effect of the half-wave plate (HWP) and the quarter-wave plate (QWP), with fast axes h and q respectively, with respect to the vertical direction are given by the matrices

$$U_{HWP} = \frac{1}{\sqrt{2}} \begin{pmatrix} \cos(2h) & -\sin(2h) \\ -\sin(2h) & -\cos(2h) \end{pmatrix}\tag{10}$$

$$U_{QWP} = \begin{pmatrix} i - \cos(2q) & \sin(2q) \\ \sin(2q) & -i + \cos(2q) \end{pmatrix}\tag{11}$$

which means that both waveplates shift the polarization of the incoming light. The HWP changes the direction of linearly polarized light, while the QWP converts linearly polarized light into circularly polarized light.

Hence, the projection state for the beam is given by

$$|\psi_{\text{proj}}(h, q)\rangle = U_{HWP} U_{QWP} |\psi_0\rangle = a(h, q) |H\rangle + b(h, q) |V\rangle,\tag{12}$$

where $|\psi_0\rangle$ is an initial arbitrarily prepared state and a and b are coefficient dependent on the configuration of the waveplates. We can denote a projection state corresponding to a particular set of waveplate angles $\{h, q\}$ by a ket $|\psi_\nu\rangle$. Hence, the average number of counts in each detector will be given by

$$n_\nu = \mathcal{N} \langle \psi_\nu | \rho | \psi_\nu \rangle, \quad (13)$$

where \mathcal{N} is a constant dependent on the laser intensity and the detector efficiency. In our setup the Stokes parameters can be defined from a set of intensity measurements (cf. section 2.3). The number of photons counted by the detectors are related to the Stokes parameters as follows:

$$\begin{aligned} S_0 &\equiv 2n_0 = \mathcal{N}(\langle H | \rho | H \rangle + \langle V | \rho | V \rangle) = 1 \\ S_1 &\equiv 2(n_1 - n_0) = \mathcal{N}(\langle D | \rho | D \rangle - \langle A | \rho | A \rangle) \\ S_2 &\equiv 2(n_2 - n_0) = \mathcal{N}(\langle L | \rho | L \rangle - \langle R | \rho | R \rangle) \\ S_3 &\equiv 2(n_3 - n_0) = \mathcal{N}(\langle H | \rho | H \rangle - \langle V | \rho | V \rangle). \end{aligned} \quad (14)$$

$$(15)$$

By means of the Stokes parameters one can write the density matrix ρ as:

$$\rho = \frac{1}{2} \left(\sum_{i=0}^3 S_i \sigma_i \right). \quad (16)$$

Thus, experimentally determining the Stokes parameters is equivalent to a *complete tomographic measurement* of the density matrix of an ensemble of single qubits.

2.3. Experimental setup

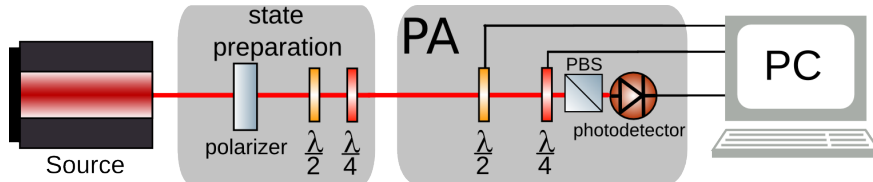


Figure 1: Experimental setup to make a QST of a single photon where $\frac{\lambda}{2}$ and $\frac{\lambda}{4}$ stands for HWP and QWP respectively.

In the first stage, we use the setup depicted in Fig.1. A 808 nm laser source is coupled to an optical fiber, then passes through a polarizer to set the polarization of the light to vertical. Thus, the initial state is ρ_V . A HWP is used to prepare the states ρ_H , ρ_A or ρ_D from the initial ρ_V ; and a QWP is used for preparing ρ_R and ρ_L (cf. section 2.2).

The Polarization Analyzer (PA) consists also of a HWP, a QWP and a polarization beam splitter (PBS), connected to an automated software in Labview that sweeps a series of angles on both HWP and QWP (as seen in Table 1) to project the prepared state in the different basis shown in Eq.(6). Finally a photo-diode measures the intensity of the light in each specific polarization for the six projected states mentioned above.

2.4. Experimental procedure and results

In Table 1 we show the required angles in both HWP and QWP to project ρ_V , in each of the states $|i\rangle$ for ($i = H, A, D, R, L$). For the other five prepared polarization states, the process is analogous.

Table 1: Angles h and q to project, in the polarization state $|i\rangle$, a vertical state ρ_V .

State	h ($^\circ$)	q ($^\circ$)
$ V\rangle$	0.0	0.0
$ H\rangle$	45.0	0.0
$ A\rangle$	22.5	0.0
$ D\rangle$	337.5	0.0
$ R\rangle$	0.0	315.0
$ L\rangle$	0.0	45.0

The software saves one data file containing 1000 intensity measurements from the photodiode, for each of the configurations in the PA, for each of the six prepared states.

By definition the Stokes parameter $S_0 = 1$, so the normalization factor, in each case, is the sum of the mean intensity for the measurement with $h = q = 0^\circ$ and its orthogonal part. Using `Mathematica` we compute the mean intensity for each measurement and calculate the normalized Stokes parameters according to Eq.(8) to reconstruct, via Eq.(16), the density matrix for the prepared state. The results of our single qubit tomographies are:

$$\rho_V^{(E)} = \begin{pmatrix} 0.005 & 0.022 - 0.217i \\ 0.023 + 0.217i & 0.995 \end{pmatrix} \pm \Delta\rho$$

$$\rho_H^{(E)} = \begin{pmatrix} 0.996 & 0.004 - 0.186i \\ 0.004 + 0.186i & 0.004 \end{pmatrix} \pm \Delta\rho$$

$$\rho_A^{(E)} = \begin{pmatrix} 0.513 & -0.485 - 0.266i \\ -0.485 + 0.266i & 0.487 \end{pmatrix} \pm \Delta\rho$$

$$\rho_D^{(E)} = \begin{pmatrix} 0.509 & 0.498 - 0.135i \\ 0.498 + 0.135i & 0.491 \end{pmatrix} \pm \Delta\rho$$

$$\rho_R^{(E)} = \begin{pmatrix} 0.498 & -0.171 + 0.493i \\ -0.171 - 0.493i & 0.500 \end{pmatrix} \pm \Delta\rho$$

$$\rho_L^{(E)} = \begin{pmatrix} 0.480 & -0.065 - 0.499i \\ -0.065 + 0.499i & 0.520 \end{pmatrix} \pm \Delta\rho$$

Where the superscript E stands for experimental results, and $\Delta\rho$ is a matrix that represents an experimental uncertainty of 0.005 computed as the average of the standard deviations of the six intensity measurements. The density matrix plots for each of the reconstructed matrices are shown in [Appendix B](#). Comparing the experimental results with Eq.(7) we see a good agreement with what is theoretically expected. Of course, there are some errors due to experimental limitations but the overall result of the tomography is successful since the tomographic reconstruction of the matrices is very accurate. However, we should note that we perceive a possible systematic error, seen in the off-diagonal elements of the imaginary part in the density matrices, which we believe has to do with a poor characterization of the waveplates used, and the possibility that they were not properly cleaned before our measurement.

3. 2-qubit quantum state tomography

3.1. Theoretical preliminaries

3.1.1. Complete tomographic measurements

As in the single qubit case we think of the projected state vector as the tensor product of each projected single qubit state

$$|\psi_{proj}(h_1, h_2, q_1, q_2)\rangle = |\psi_{proj}(h_1, q_1)\rangle \otimes |\psi_{proj}(h_2, q_2)\rangle. \quad (17)$$

We will define a ket $|\psi_\nu\rangle$ as the result of the ν -th projective measurement corresponding to a particular combination of the 4 waveplate angles $\{h_1, h_2, q_1, q_2\}$. Consequently, the average number of photon counts observed in our setup will be

$$n_\nu = \mathcal{N} \langle \psi_\nu | \rho | \psi_\nu \rangle, \quad (18)$$

where ρ is the density matrix representing the photonic ensemble being tomographed and \mathcal{N} is a constant dependent on the intensity of the light and the detectors efficiency.

Analogous to the case of a single qubit where the density matrix could be written as a certain linear combination of the Pauli matrices, cf. Eq.(16), (which means that the appropriate Hilbert space is $SU(2)$), the two-qubit case can be thought of as taking two copies of single qubit Hilbert spaces each representing one of the qubits in the pair. Thus, the Hilbert space that is of interest is $\mathcal{H} = SU(2) \otimes SU(2)$. This Hilbert space is spanned by the 16 2-qubit Pauli matrices $\sigma_i \otimes \sigma_j$ ($i, j = 0, 1, 2, 3$). Using this 16 matrices, Γ_ν ($\nu = 1, \dots, 16$), as the basis of \mathcal{H} , any two-qubit density matrix can be written as

$$\rho = \sum_{\nu=1}^{16} \Gamma_\nu x_\nu, \quad (19)$$

where x_ν is the ν -th component of the vector

$$x_\nu = \text{tr}(\Gamma_\nu \rho). \quad (20)$$

However, this *canonical* representation of ρ is not adapted to express the density matrix in terms of quantities we can determine experimentally. To this end we must select an appropriate basis of \mathcal{H} , allowing us to reconstruct the density matrix of the ensemble with the photon counts n_ν we measured in the laboratory. The appropriate basis in which we should write our density matrix is known as the *tomographic basis* [7]. In this basis, spanned by matrices M_μ ($\mu = 1, \dots, 16$), the density matrix is written as

$$\rho = \frac{\sum_{\mu=1}^{16} M_\mu n_\mu}{\sum_{\mu=1}^4 n_\mu} \quad (21)$$

for the full mathematical details of how to construct the tomographic basis see [Appendix A](#).

3.1.2. Physical density matrix

We should emphasize that the density matrix Eq.(21) as constructed previously is by construction Hermitian, i.e. $\rho^\dagger = \rho$, and normalized, i.e. $\text{tr}(\rho) = 1$. However, such a construction can not enforce the matrix to be positive-definite, i.e. that all its eigenvalues are strictly positive¹. And since any density matrix for physical states must be a positive-definite matrix the linear reconstruction described in the previous section to obtain a density matrix from coincidence counts is not appropriate, as the tomographic reconstruction violates the positivity of physical density matrices. As commented in [7] this violation of positivity happens roughly 75% of the time for low entropy highly *entangled states*. Hence, we must resort to a *maximum likelihood estimation* in order to find a physical density matrix describing our photonic ensemble compatible with the experimental measurements.

Let us describe how to construct a physical density matrix. Any matrix M is positive-definite if

$$\langle \psi | M | \psi \rangle \geq 0 \quad (22)$$

for all $|\psi\rangle \neq \vec{0}$. Furthermore, any matrix that can be written in the form $M = T^\dagger T$ must be positive definite since

$$\langle \psi | M | \psi \rangle = \langle \psi | T^\dagger T | \psi \rangle \geq 0. \quad (23)$$

Also, since $M^\dagger = (T^\dagger T)^\dagger = T^\dagger T = M$, the matrix M is Hermitian. Obtaining a normalized matrix from M is straightforward since it amounts only to divide by its trace, viz

$$\rho_p = \frac{T^\dagger T}{\text{tr}(T^\dagger T)}. \quad (24)$$

Hence, ρ_p has all three properties that characterize a physical density matrix and thus, is a valid parametrization for physical density matrices. For a 2-qubit system, we have a 4×4 with 16 independent real parameter. Thus, we can parameterize matrix T as [7]:

¹since the eigenvalues of a density matrix represent probabilities they must all be positive.

$$T(t_1, \dots, t_{16}) = \begin{pmatrix} t_1 & 0 & 0 & 0 \\ t_5 + it_6 & t_2 & 0 & 0 \\ t_{11} + it_{12} & t_7 + it_8 & t_3 & 0 \\ t_{15} + it_{16} & t_{13} + it_{14} & t_9 + it_{10} & t_4 \end{pmatrix}, \quad (25)$$

with the t_i 's real. With these parametrization we can obtain an explicit form for the physical density matrix, ρ_p , in terms of $T(t)$ simply as

$$\rho_p = \frac{T(t)^\dagger T(t)}{\text{tr}(T(t)^\dagger T(t))} \quad (26)$$

where $t = \{t_i\}_{i=1, \dots, 16}$.

3.1.3. Maximum likelihood estimation

The experimental data consists of 16 coincidence measurements, n_ν , with expected value $\langle n_\nu \rangle = \mathcal{N} \langle \psi_\nu | \rho | \psi_\nu \rangle$. If we assume that the coincidence measurements are independent and normally distributed, the probability of obtaining a set of 16 measurements is given by

$$\mathcal{P}(n_\nu) = \frac{1}{Z} \prod_{\nu=1}^{16} \exp\left(-\frac{(n_\nu - \langle n_\nu \rangle)^2}{2\sigma_\nu^2}\right), \quad (27)$$

where Z is an appropriate normalization constant and $\sigma_\nu = \sqrt{\langle n_\nu \rangle}$ is the standard deviation for the ν -th measurement. In terms of our parametrization of the physical density matrix, ρ_p , the expected number of coincidences is

$$\langle n_\nu(t_1, \dots, t_{16}) \rangle = \mathcal{N} \langle \psi_\nu | \rho_p(t_1, \dots, t_{16}) | \psi_\nu \rangle. \quad (28)$$

Hence, the likelihood that ρ_p produced the measured data is:

$$\mathcal{P}(t_1, \dots, t_{16}) = \frac{1}{Z} \prod_{\nu=1}^{16} \exp\left(-\frac{(n_\nu - \mathcal{N} \langle \psi_\nu | \rho_p(t_1, \dots, t_{16}) | \psi_\nu \rangle)^2}{2\mathcal{N} \langle \psi_\nu | \rho_p(t_1, \dots, t_{16}) | \psi_\nu \rangle}\right), \quad (29)$$

thus, we need to find the maximum value of $\mathcal{P}(t_1, \dots, t_{16})$ which will tell us the most probable set of parameters t_i , and thus the most probable density matrix given our 16 coincidence measurements. However, it is easier to maximize the logarithm of (29), which is equivalent to *minimizing* the function

$$\Lambda(t_1, \dots, t_{16}) = \sum_{\nu=1}^{16} \frac{(n_\nu - \mathcal{N} \langle \psi_\nu | \rho_p(t_1, \dots, t_{16}) | \psi_\nu \rangle)^2}{2\mathcal{N} \langle \psi_\nu | \rho_p(t_1, \dots, t_{16}) | \psi_\nu \rangle}. \quad (30)$$

We minimized this function numerically in order to find the set of parameters $\{t_\nu\}_{\nu=1, \dots, 16}$, which we will use to reconstruct a valid physical density matrix using Eq.(26).

3.2. Experimental setup

In the second stage, we use the setup depicted in Fig.2.

- Source: A CrystaLaser source of 405 nm with a bandwidth of 5 nm.
- BBO Crystal: An EKSMA BBO colinear crystal with type II phase matching of thickness 4 mm to produce a pair of SPDC photons with double the wavelength of the source light and mutually orthogonal polarizations.
- A dichroic mirror is used to reflect the pump of the laser (405 nm), the SPDC photons pass through it.
- PBS: A polarization beamsplitter divides the horizontal polarization into *path A* and vertical polarization into *path B*.
- BS: A beamsplitter or power-splitter divides by half the power of the incident light into *path A* and *path B*.
- HWP and QWP: A pair of waveplates (HWP and QWP) is used in each polarization analyzer to project the prepared state in the tomographic basis. The half-wave plates are motorized and connected to a software; the quarter-wave plates are manually manipulated.
- Photodetector: A PerkinElmer single photon counting module (SPCM-ARQ).
- FPGA: The photodetectors are connected to a field-programmable gate array (FPGA) which receives their signals and shows the number of coincidence counts².

3.3. Experimental procedure and results

First, we characterize the 4 waveplates used in the PA's by setting their respective fast axes to *zero*. We compared the number of coincidence counts in the photodetectors with and without the waveplates in the PA, looking for the angles that produce the same coincidences. After finding these angles we proceeded to compare the waveplate behavior (by sweeping their angles) with what is expected from Eqs.(10),(11).

3.3.1. Quantum state tomography using a PBS

In order to test our experimental setup we used a polarization beamsplitter (PBS) to divide the horizontal polarization into *path A* and vertical into *path B*. The recipe in Table 2 is used to project the prepared state, $|H\rangle_A \otimes |V\rangle_B \equiv |HV\rangle$, in the tomographic basis. The coincidence counts n_ν are used to calculate, via Eq.(A.3), the (non-physical) density matrix of the system.

Subsequent to this we used the routine `NMinimize` in `Mathematica` to find the optimal parameters t_i in Eq.(30) where the likelihood function, $\Lambda(t)$, is a minimum. We then reconstructed the physical density matrix of the system as described in section 3.1. In Fig.3 we plot the experimental results both for the real and imaginary parts of the density matrix which correspond to the prepared state using the PBS:

²A coincidence is a count in both detectors, that occur within a time window of 9 ns.

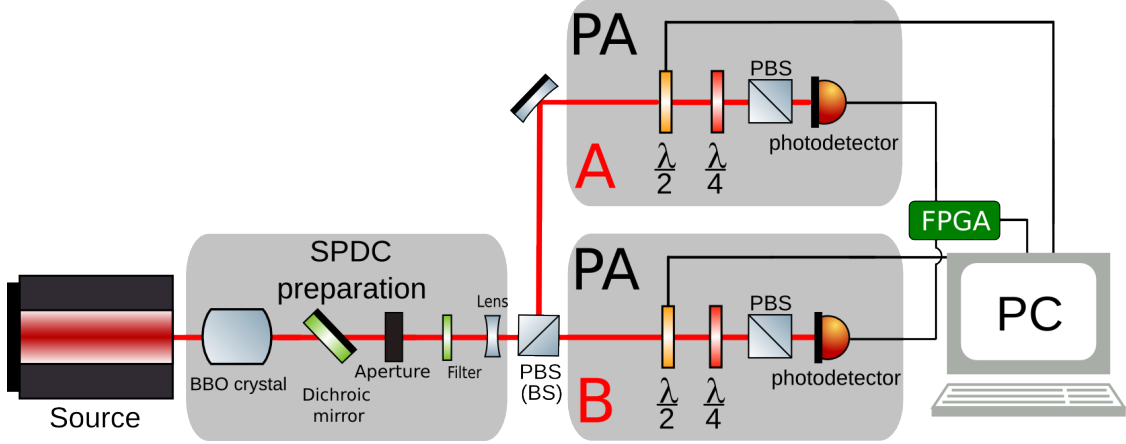


Figure 2: Experimental setup for the 2 qubit quantum state tomography. *State preparation*: A laser of 405 nm passes through a Type II BBO Crystal to produce entangled pairs of photons. A dichroic mirror is used to get rid of the pump of the laser. Then, an aperture is used to align the light, the filter further filters the remaining 405 nm pump and finally a lens properly collimates the SPDC light into the PBS (BS) that separates the photons into path A or B. *PA*: In each path we have the same polarization analyzer consisting of a motorized HWP ($\lambda/2$) and a manual QWP ($\lambda/4$) followed by a PBS and coupled to a multimode optical fiber, finally a single photon detector is connected to a computer to store the data.

Table 2: Experimental procedure to project the prepared state into the 16 states of the tomographic basis. h_A and q_A stand for the angles in the HWP and QWP respectively in the *path A*, analogous for *path B*.

ν	Mode A	Mode B	h_A ($^\circ$)	q_A ($^\circ$)	h_B ($^\circ$)	q_B ($^\circ$)
1	$ H\rangle$	$ H\rangle$	45.0	0.0	45.0	0.0
2	$ H\rangle$	$ V\rangle$	45.0	0.0	0.0	0.0
3	$ V\rangle$	$ V\rangle$	0.0	0.0	0.0	0.0
4	$ V\rangle$	$ H\rangle$	0.0	0.0	45.0	0.0
5	$ R\rangle$	$ H\rangle$	22.5	0.0	45.0	0.0
6	$ R\rangle$	$ V\rangle$	22.5	0.0	0.0	0.0
7	$ D\rangle$	$ V\rangle$	22.5	45.0	0.0	0.0
8	$ D\rangle$	$ H\rangle$	22.5	45.0	45.0	0.0
9	$ D\rangle$	$ R\rangle$	22.5	45.0	22.5	0.0
10	$ D\rangle$	$ D\rangle$	22.5	45.0	22.5	45.0
11	$ R\rangle$	$ D\rangle$	22.5	0.0	22.5	45.0
12	$ H\rangle$	$ D\rangle$	45.0	0.0	22.5	45.0
13	$ V\rangle$	$ D\rangle$	0.0	0.0	22.5	45.0
14	$ V\rangle$	$ L\rangle$	0.0	0.0	22.5	90.0
15	$ H\rangle$	$ L\rangle$	45.0	0.0	22.5	90.0
16	$ R\rangle$	$ L\rangle$	22.5	0.0	22.5	90.0

$$\rho_P^{\text{PBS}} = \begin{pmatrix} 0.003 & -0.006 - 0.050i & -0.000 + 0.000i & -0.001 - 0.001i \\ -0.006 + 0.050i & 0.991 & -0.006 - 0.008i & 0.030 - 0.021i \\ -0.000 - 0.000i & -0.006 + 0.008i & 0.000 & 0.000 + 0.000i \\ -0.001 + 0.001i & 0.030 + 0.021i & 0.000 - 0.000i & 0.006 \end{pmatrix}.$$

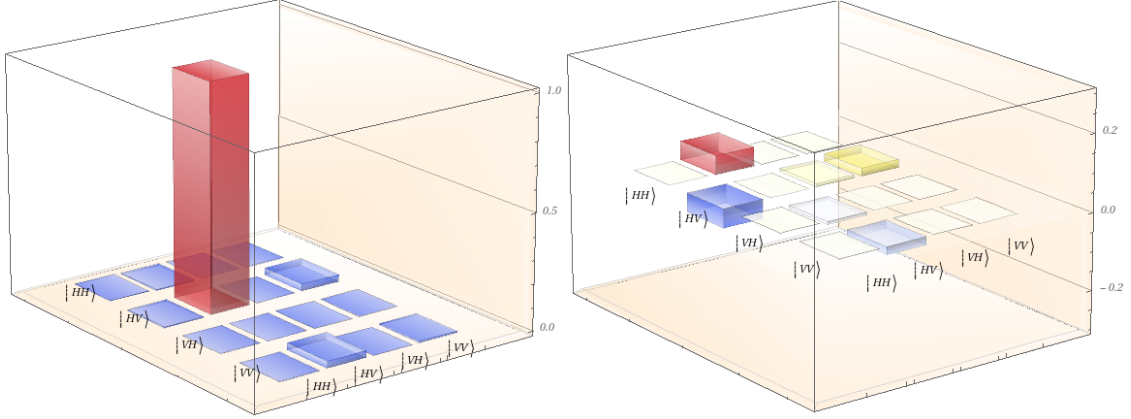


Figure 3: Real part (right) and imaginary part (left) of the physical density matrix corresponding to the state $|HV\rangle$.

3.3.2. Quantum state tomography using a BS

This setup is analogous to the one described in the previous section, but replacing the PBS for a beamsplitter (BS). A BS divides roughly by a half the power of incident light (rather than its polarization components) into the paths A and B . Hence, with this setup, we theoretically expect to prepare the ensemble in a *pure state* of the form

$$|\psi_{\text{expected}}\rangle = \frac{1}{\sqrt{2}}(|HV\rangle + e^{i\phi}|VH\rangle), \quad (31)$$

where ϕ is a phase factor due to phase matching conditions, temporal and spatial separation [8]. The state in Eq.(31) corresponds to the density matrix

$$\rho_{\text{expected}} = \begin{pmatrix} 0 & 0 & 0 & 0 \\ 0 & 1/2 & 1/2 & 0 \\ 0 & 1/2 & 1/2 & 0 \\ 0 & 0 & 0 & 0 \end{pmatrix}. \quad (32)$$

After the pair of photons passes the BS we use the recipe in Table 2 to project the state in the tomographic basis. Again we calculated the physical density matrix of the system using *Mathematica*, being

$$\rho_{\text{P}}^{\text{BS}} = \begin{pmatrix} 0.021 & -0.020 - 0.008i & 0.004 + 0.014i & -0.010 + 0.009i \\ -0.020 + 0.008i & 0.515 & -0.009 + 0.001i & -0.007 - 0.019i \\ 0.004 - 0.014i & -0.009 - 0.001i & 0.435 & 0.017 + 0.001i \\ -0.010 - 0.009i & -0.007 + 0.019i & 0.017 - 0.001i & 0.029 \end{pmatrix},$$

which is plotted in Fig.4. We note that the reconstructed density matrix resembles a maximally *mixed state* density matrix of the form

$$\rho_{\text{T}} = \frac{1}{2}(|HV\rangle\langle HV| + |VH\rangle\langle VH|) = \begin{pmatrix} 0 & 0 & 0 & 0 \\ 0 & 1/2 & 0 & 0 \\ 0 & 0 & 1/2 & 0 \\ 0 & 0 & 0 & 0 \end{pmatrix}, \quad (33)$$

rather than a *pure state*. A density matrix like the one reconstructed in Fig.4 exhibits *distinguishability* between the SPDC photons after passing through the BS, that is, destruction of the coherences in the system. This is a consequence of a temporal separation, Δt , between the pair of photons produced within the BBO crystal. We tried to overcome this handicap by compensating this delay using another BBO crystal as we will describe shortly.

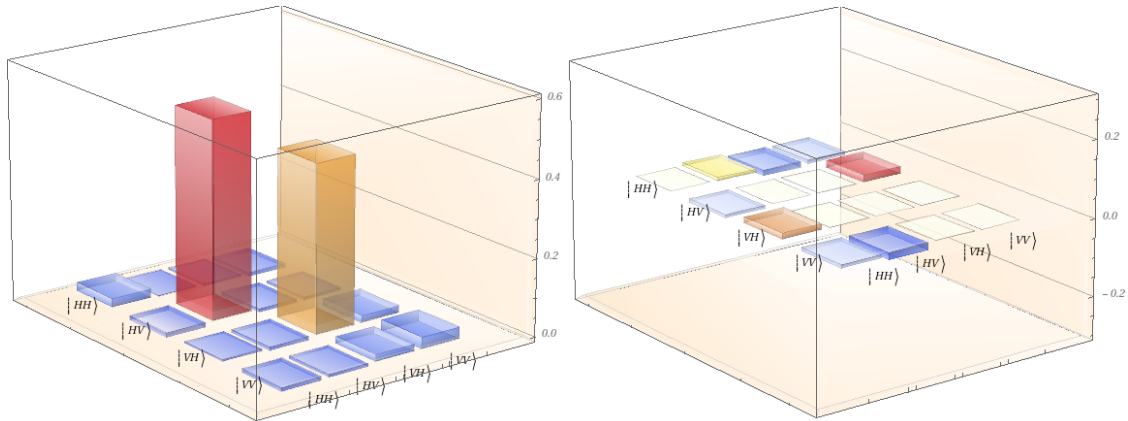


Figure 4: Real part (right) and imaginary part (left) of the reconstructed physical density matrix.

In quantum information theory, the fidelity, \mathcal{F} , is a measure of the *closeness* of two quantum states, ρ_1 and ρ_2 , [9], and it is defined as

$$\mathcal{F}(\rho_1, \rho_2) = \text{tr} \left(\sqrt{\sqrt{\rho_1} \rho_2 \sqrt{\rho_1}} \right), \quad (34)$$

where a fidelity of 0 means that the states do not resemble at all, and a fidelity of 1 means the two states are the same. The fidelity between the experimental results ρ_p^{BS} and the theoretical matrix ρ_T is: $\mathcal{F}(\rho_p^{\text{BS}}, \rho_T) = 0.974$, which means the reconstructed density matrix is very *close* to the theoretical density matrix. Taking the partial trace of ρ_T results in a 2×2 matrix that is proportional to the identity matrix, which implies it is a maximally *entangled state*. Given that the fidelity is close to 1, we can say the tomographically reconstructed density for the SPDC source represents a *mixed, entangled state*.

3.3.3. Temporal separation compensation

A BBO Crystal is an uniaxial crystal that has a specific direction called the optical axis. When the pair of photons is produced, the one polarized in the plane formed by the propagation vector and the optical axis is called extraordinary (e-polarized), the photon polarized normal to this plane is said to be ordinary (o-polarized) [8]. The group velocity (that depends on the refractive index) is then different for e-polarized and o-polarized photons leading to an average arrival delay between the produced pair. If the temporal separation between the pair of photons produced in the BBO Crystal is larger than the coherence time of the laser, it can lead to decoherence of the entangled two-photon states. To compensate this effect one has to add a second BBO Crystal (compensation crystal), whose optical axis is orthogonal to the first crystal. This means that the e-polarized photon produced by the first crystal is now o-polarized for the compensation crystal and vice-versa. Hence, by this compensation, the temporal separation is corrected.

In our setup (cf. Fig.2) we placed, between the dichroic mirror and the aperture, a 2 mm thick type II BBO-Crystal with 5° of half-open angle. Since the second BBO crystal is not colinear³, we had to tilt it with respect to the colinear one to be able to compensate the temporal delay [1]. However, attempting the compensation of a colinear crystal with a non-colinear one is neither simple nor ideal, since the tilting may cause further unwanted effects in the polarization state of the ensemble. The ideal procedure to compensate the temporal delay is by using a compensation crystal with half the thickness of the first crystal and the same half-open angle [1]. Nevertheless, due to laboratory availability we did not possess a crystal with the ideal characteristics for the compensation procedure.

Analogous to the previous case, the reconstructed physical density matrix of the system (with the compensation crystal) is

$$\rho_p^{\text{BS-C}} = \begin{pmatrix} 0.037 & 0.000 - 0.036i & 0.024 - 0.031i & -0.009 - 0.007i \\ 0.000 + 0.036i & 0.495 & 0.005 + 0.004i & -0.022 + 0.061i \\ 0.024 + 0.031i & 0.005 - 0.004i & 0.446 & -0.006 + 0.037i \\ -0.009 + 0.007i & -0.027 - 0.061i & -0.006 - 0.037i & 0.023 \end{pmatrix}.$$

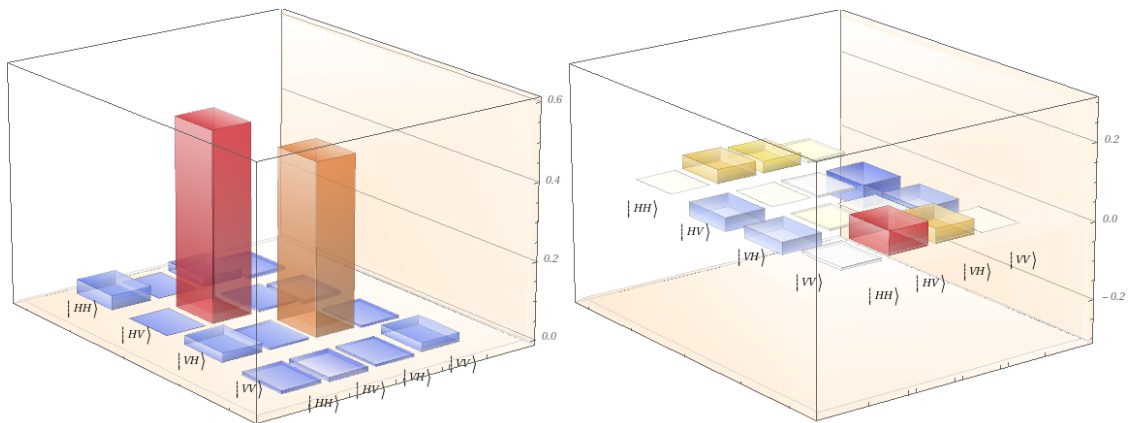


Figure 5: Real part (right) and imaginary part (left) of the reconstructed physical density matrix.

In Fig.5 we show graphically the corresponding density matrix after attempting the compensation. It again resembles the *mixed state* Eq.(33) rather than the *pure state* we expect after compensating the temporal delay. Note that some of the imaginary components of $\rho_p^{\text{BS-C}}$ got bigger and the off-diagonal terms (coherences) we expected to correct, according to Eq.(32), remained the same. This result can be understood as a consequence of using a non-colinear compensation crystal and trying to tilt it with respect to the first crystal. This means the phase factor in Eq.(31) may not be corrected by this procedure, but on the contrary, the phase matching can be affected leading to another unwanted phase causing decoherence [8]. Furthermore, due to the tilting, the distance traveled by the light inside the compensation crystal is not exactly 2 mm, which can result in further temporal separation. Hence, our attempt at the time delay compensation without another colinear crystal was unsuccessful, and we did not obtain the expected pure state.

³Colinear crystals have 0° of half-open angle.

4. Conclusions

In this document, we present the implementation and results of single and two-qubit quantum state tomography. For the single qubit experiment we used a laser source and a set of waveplates to prepare the polarization state of the source in six different states corresponding to the *vertical*, *horizontal*, *diagonal*, *antidiagonal*, *right* and *left* polarizations. By means of a single qubit quantum state tomography, we successfully reconstructed the density matrix for the six polarization states of the three different polarization bases, which were compared to the theoretical predictions obtaining good agreement.

For the two-qubit tomography, we used SPDC photons produced in a type II BBO crystal and implement two-qubit quantum state tomography based on measuring the James-Kwiat-Munro-White projectors for the down-converted photons. We made two different tomographies, using both a BS and a PBS after the SPDC source. Based on [1] and the requirement of positivity for density matrices we programmed a maximum likelihood estimation routine to reconstruct the (physical) density matrix for the ensemble of SPDC photons. After the tomographic reconstruction of the 2-qubit density matrix we computed its *fidelity* with a mixed, entangled density matrix and obtained a value of $\mathcal{F} = 0.974$, which tells us that our experimentally reconstructed density matrix represents a mixed ensemble of two entangled qubits. However, due to the temporal separation induced by the nonlinear crystal in the pair of down-converted photons, we could not prepare the state of the ensemble in the desired *pure state*. And due to laboratory equipment unavailability, the proper time compensation of the type II BBO colinear crystal was not possible during this project. However, the tomographic reconstruction of an entangled 2-qubit SPDC photonic ensemble was successful.

Acknowledgement

The authors would like to thank the quantum optics group at Universidad de Los Andes and our project director Mayerlin Nuñez for their guidance and support during this project. We especially would like to thank Omar Calderón, Daniel Urrego, Victor Buesaquillo, John Fredy Suárez for their help in the laboratory and the useful discussions that helped us better understand the theoretical details involved in the development of this project.

References

- [1] P. G. Kwiat, E. Waks, A. G. White, I. Appelbaum, P. H. Eberhard, [Ultrabright source of polarization-entangled photons](#), Phys. Rev. A 60 (1999) R773–R776. doi:10.1103/PhysRevA.60.R773. URL <https://link.aps.org/doi/10.1103/PhysRevA.60.R773>
- [2] U. Fano, Description of states in quantum mechanics by density matrix and operator techniques, Rev. Mod. Phys. 29 (1957) 74–93. doi:10.1103/RevModPhys.29.74.
- [3] K. Vogel, H. Risken, Determination of quasiprobability distributions in terms of probability distributions for the rotated quadrature phase, Phys. Rev. A 40 (1989) 2847–2849. doi:10.1103/PhysRevA.40.2847.
- [4] U. Leonhardt, Quantum-state tomography and discrete wigner function, Phys. Rev. Lett. 74 (1995) 4101–4105. doi:10.1103/PhysRevLett.74.4101.
- [5] M. Beck, Quantum Mechanics. Theory and experiment, Oxford University Press, 2012.
- [6] J. Altepeter, E. Jeffrey, P. Kwiat, Photonic state tomography, http://research.physics.illinois.edu/QI/Photonics/tomography-files/amo_tomo_chapter.pdf (2004).

- [7] D. F. V. James, P. G. Kwiat, W. J. Munro, A. G. White, [Measurement of qubits](#), Phys. Rev. A 64 (2001) 052312. doi: 10.1103/PhysRevA.64.052312. URL <https://link.aps.org/doi/10.1103/PhysRevA.64.052312>
- [8] M. Schäffer, Two-photon polarization entanglement in type i spdc experiment (2009).
- [9] S. Barnett, Quantum Information (Oxford Master Series in Physics: Atomic, Optical, and Laser Physics), 2009.

AppendixA. Theoretical details

Combining Eq.(18) and Eq.(19) we obtain

$$n_\nu = \mathcal{N} \sum_{\mu=1}^{16} \langle \psi_\nu | \Gamma_\mu | \psi_\nu \rangle x_\mu. \quad (\text{A.1})$$

Provided that matrix $\langle \psi_\nu | \Gamma_\mu | \psi_\nu \rangle$ is invertible we can invert Eq.(A.1) to solve for x_μ having a complete set of tomographic states $\{\psi_\nu\}_{\nu=0,\dots,16}$ ⁴, viz

$$x_\mu = \frac{1}{\mathcal{N}} \sum_{\nu=1}^{16} (\langle \psi_\nu | \Gamma_\mu | \psi_\nu \rangle)^{-1} n_\nu. \quad (\text{A.2})$$

These states are the result of setting specific values for the angles of the waveplates in the polarization analyzers. Using Eq.(A.2) we can rewrite Eq.(19) as

$$\rho = \frac{1}{\mathcal{N}} \sum_{\mu=1}^{16} \Gamma_\mu (\langle \psi_\nu | \Gamma_\mu | \psi_\nu \rangle)^{-1} n_\mu = \frac{1}{\mathcal{N}} \sum_{\mu=1}^{16} M_\mu n_\mu, \quad (\text{A.3})$$

where we have defined the 4×4 matrix $M_\mu \equiv \Gamma_\mu (\langle \psi_\nu | \Gamma_\mu | \psi_\nu \rangle)^{-1}$. To determine the value of \mathcal{N} we can use the fact that

$$\mathcal{N} = \sum_{\mu} \text{tr}(M_\mu) n_\mu, \quad (\text{A.4})$$

and that for the set of projective measurements we used

$$\sum_{\mu} \text{tr}(M_\mu) = \begin{cases} 1 & \text{if } \mu = 1, 2, 3, 4 \\ 0 & \text{if } \mu = 5, \dots, 16 \end{cases}, \quad (\text{A.5})$$

hence, \mathcal{N} is given simply by

$$\mathcal{N} = \sum_{\mu}^4 n_\mu \quad (\text{A.6})$$

AppendixB. Single qubit density matrices

In this appendix, we show the respective matrix plots for the six reconstructed density matrices.

⁴Overall phase factors do not affect the results of projective measurements.

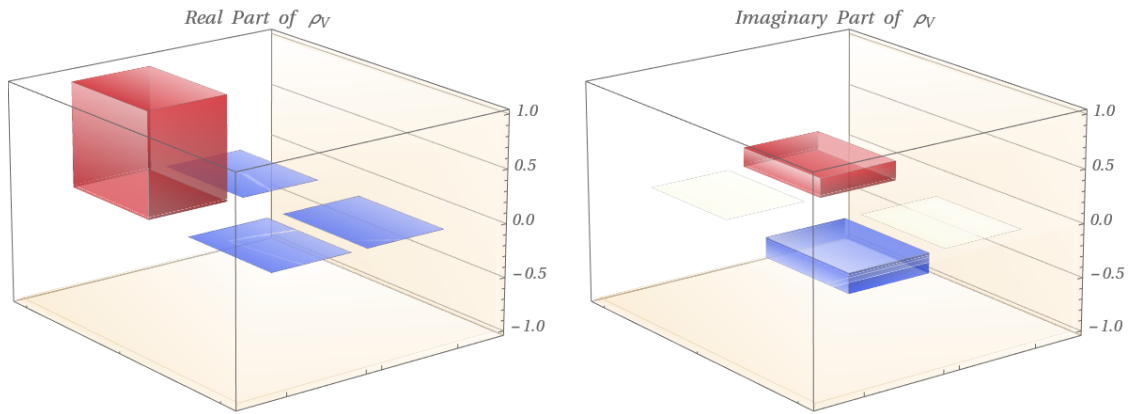


Figure B.6: Real part (right) and imaginary part (left) of the reconstructed density matrix for a *vertical* state ρ_V .

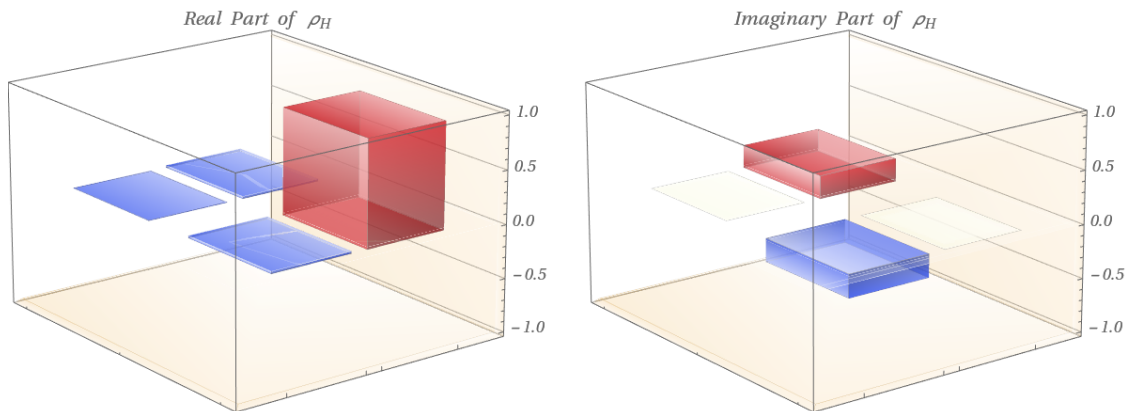


Figure B.7: Real part (right) and imaginary part (left) of the reconstructed density matrix for a *horizontal* state ρ_H .

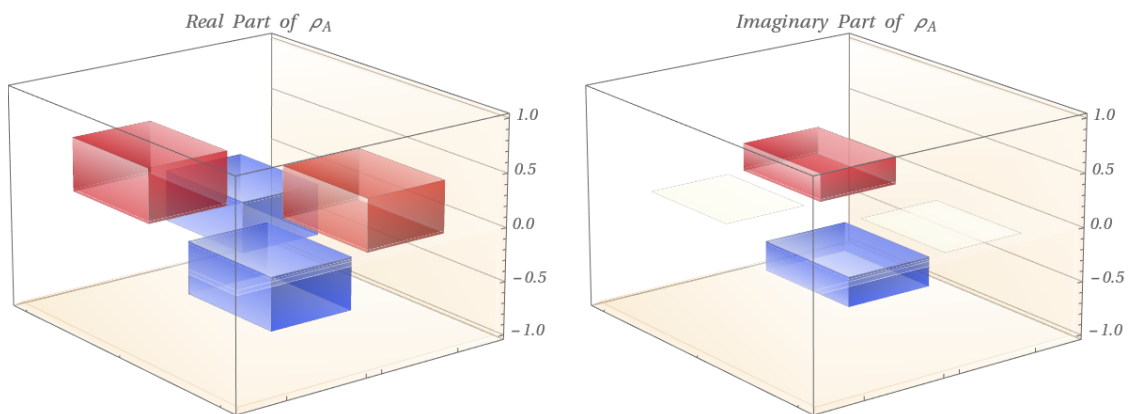


Figure B.8: Real part (right) and imaginary part (left) of the reconstructed density matrix for an *antidiagonal* state ρ_A .

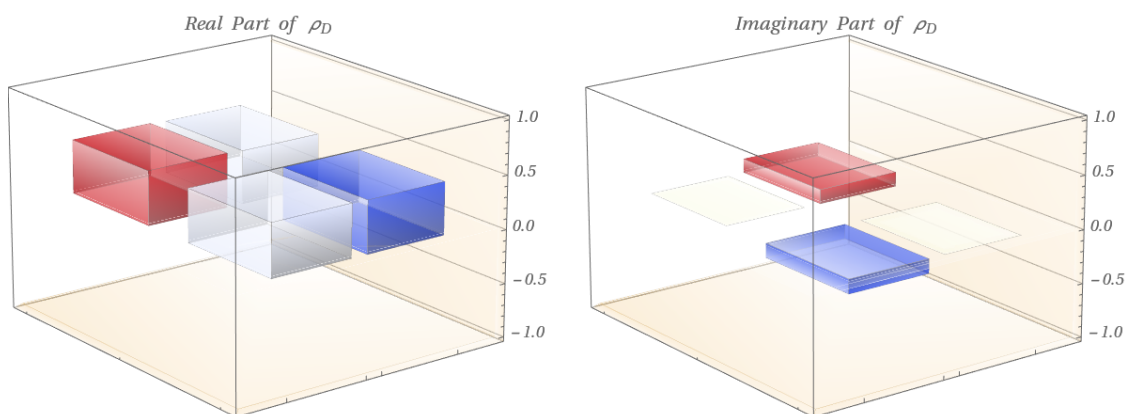


Figure B.9: Real part (right) and imaginary part (left) of the reconstructed density matrix for a *diagonal* state ρ_D .

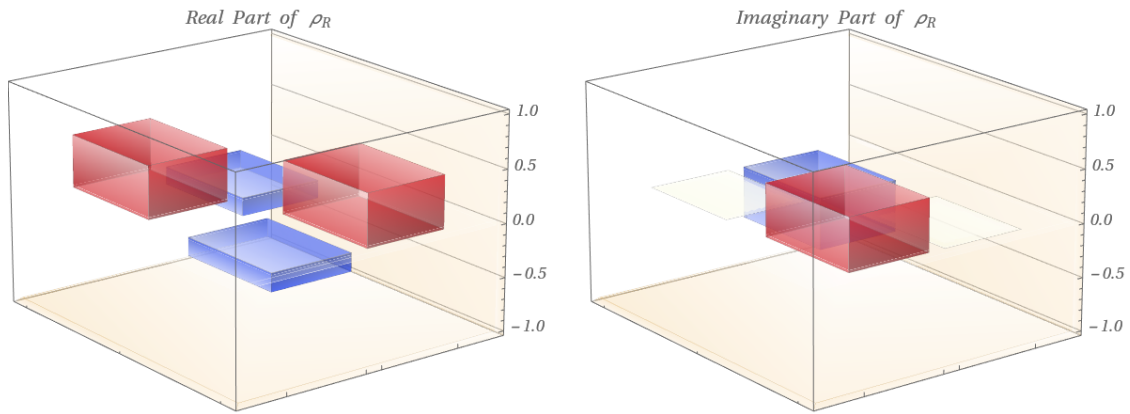


Figure B.10: Real part (right) and imaginary part (left) of the reconstructed density matrix for a *right* state ρ_R .

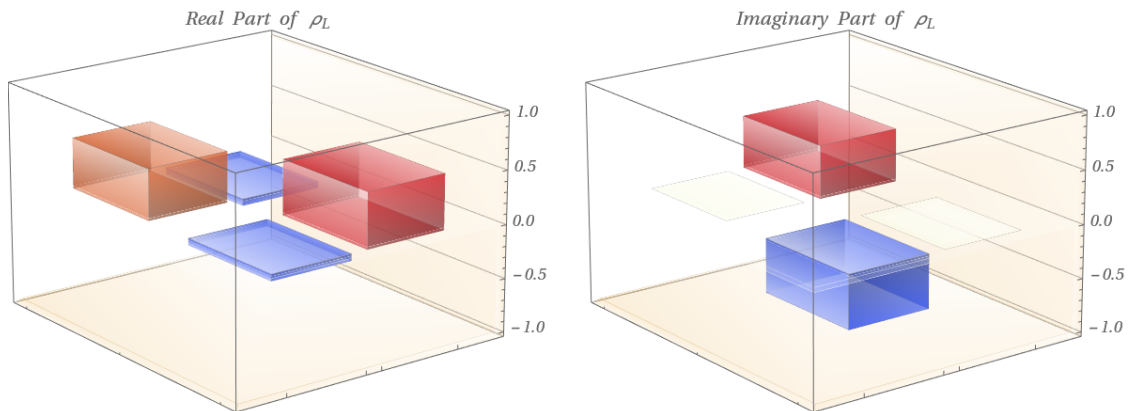


Figure B.11: Real part (right) and imaginary part (left) of the reconstructed density matrix for a *left* state ρ_L .